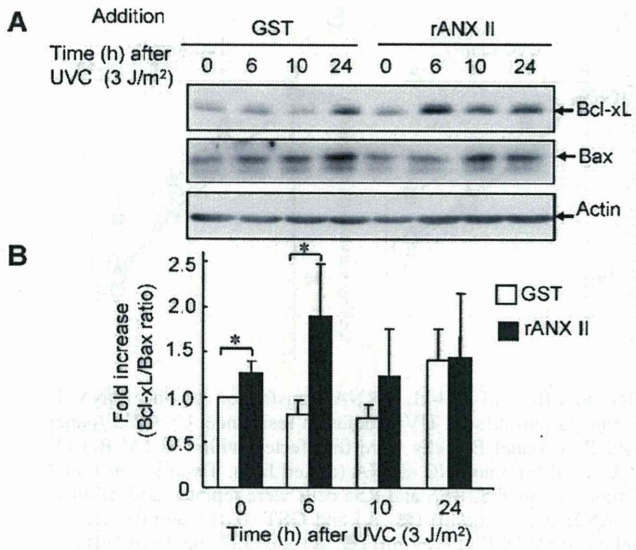

FIG. 4. Expression of Bcl-xL and Bax proteins after UVC irradiation in rANX II-supplemented CS3BES cells. CS3BES cells were cultured in the presence of rANX II (0.5 μg/ml) and GST (0.017 μg/ml) for 24 h and then irradiated with UVC light (3 J/m^2). At the indicated times after UVC irradiation, whole cell lysates were prepared, and the expression levels of Bcl-xL, Bax and actin proteins were analyzed by immunoblotting, as described in the Materials and Methods (panel A). The results shown are representative of findings from three independent experiments. Protein levels of Bcl-xL and Bax were normalized to actin levels and are presented as the ratios of Bcl-xL to Bax (panel B). The ratios immediately (time 0) after UVC irradiation in the control cells (GST alone) are designated as 1. The data are presented as means ± SD. * indicates significant difference at $P < 0.05$ for rANX II addition compared to GST control.

an increased ability to remove (6-4) photoproducts or cyclobutane pyrimidine dimers relative to their respective control cells (Fig. 3B and C). The amounts of (6-4) photoproducts and cyclobutane pyrimidine dimers immediately after irradiation (shown as time 0) were almost identical (data not shown) in the precultured and control cells.

Next, we examined the effects of a preculture with rANX II on XP cells, which are deficient in nucleotide excision repair (NER). The removal of (6-4) photoproducts and cyclobutane pyrimidine dimers was absent or low in the two XP cell lines, XP2OS and XP6BES (data not shown). After preculture with rANX II, both XP cell lines had an increased resistance to UVC-radiation-induced cell death (Fig. 3D and E). We subsequently examined the effect of XPA knockdown on the rANX II-induced radiation resistance of AP^r-1 cells, which have a higher resistance than do the CS3BES, RSa and XP cells. Knockdown of XPA (Supplementary Fig. 3A; http://dx.doi.org/10.1667/RR2561.1.S1) sensitized the AP^r-1 cells to UVC-radiation-induced cell death; this phenomenon was shown by a comparison between transfection with XPA siRNA and NC siRNA in AP^r-1 cells supplemented with control GST (Fig. 3F). There was a greater increase in resistance to UVC radiation by rANX II supplementation in the XPA-downregulated AP^r-1 cells than in the NC siRNA-transfected cells, but an increase was still observed in NC siRNA-transfected cells (Fig. 3F). However, an increase in resistance to UVC radiation by rANX II supplementation was observed in the XPA-siRNA treated HeLa cells but not in the NC siRNA-transfected cells (Supplementary Fig. 3A and B; http://dx.doi.org/10.1667/RR2561.1.S1).

These results suggest that the rANX II-induced resistance to UVC radiation is independent of removal of radiation-damaged DNA.

Increased Ratios of Bcl-xL to Bax after rANX II Supplementation

The amounts of an anti-apoptotic protein, Bcl-xL, and a pro-apoptotic protein, Bax, were analyzed by immunoblotting in CS3BES cells that were precultured with rANX II for 24 h and irradiated with UVC light. An increase in the expression of the Bcl-xL protein was observed from 6 h until 24 h after UVC irradiation (3 J/m^2) in the rANX II (0.5 μg/ml)-supplemented cells (Fig. 4A). In the control cells supplemented with GST, no significant increase in the amount of Bcl-xL was detected for up to 10 h after UVC irradiation, but an increase was observed 24 h after UVC irradiation (Fig. 4A). The expression of the Bax protein increased after UVC irradiation in both GST- and rANX II-supplemented cells (Fig. 4A). In the rANX II-supplemented cells, the increase in the Bax expression was slower than that in Bcl-xL expression. When the Bcl-xL to Bax protein ratios were calculated as an index of survival activity, the ratio in the rANX II-supplemented cells 6 h after UVC irradiation increased approximately 2- to 2.5-fold relative to the ratio in the control cells (Fig. 4B). The ratio was also higher in the rANX II-supplemented cells immediately after UVC irradiation (time 0; Fig. 4B). The increase in the Bcl-xL to Bax protein ratios was also observed after UVC irradiation at 6 J/m^2 in the rANX II-supplemented CS3BES cells (data not shown). The increase in the Bcl-xL to Bax protein ratios after rANX II supplementation was also observed in RSa and AP^r-1 cells (Supplementary Fig. 4; http://dx.doi.org/10.1667/RR2561.1.S1); these cells also showed an increased resistance to UVC radiation after rANX II supplementation (Fig. 3A and F).

Suppression of the rANX II Supplementation-Induced UVC-Radiation Resistance is Associated with Decreased Bcl-x to Bax Ratios by a PI3K Inhibitor and Downregulation of Bcl-xL

We then examined whether signal transduction pathways are involved in the rANX II supplementation-induced resistance to UVC radiation in CS3BES cells. When the cells were precultured with rANX II (0.5 μg/ml) in the presence of the PI3K inhibitor LY294002 (50 μ*M*), the increase in resistance to UVC radiation induced by rANX II supplementation was completely suppressed (Fig. 5A).

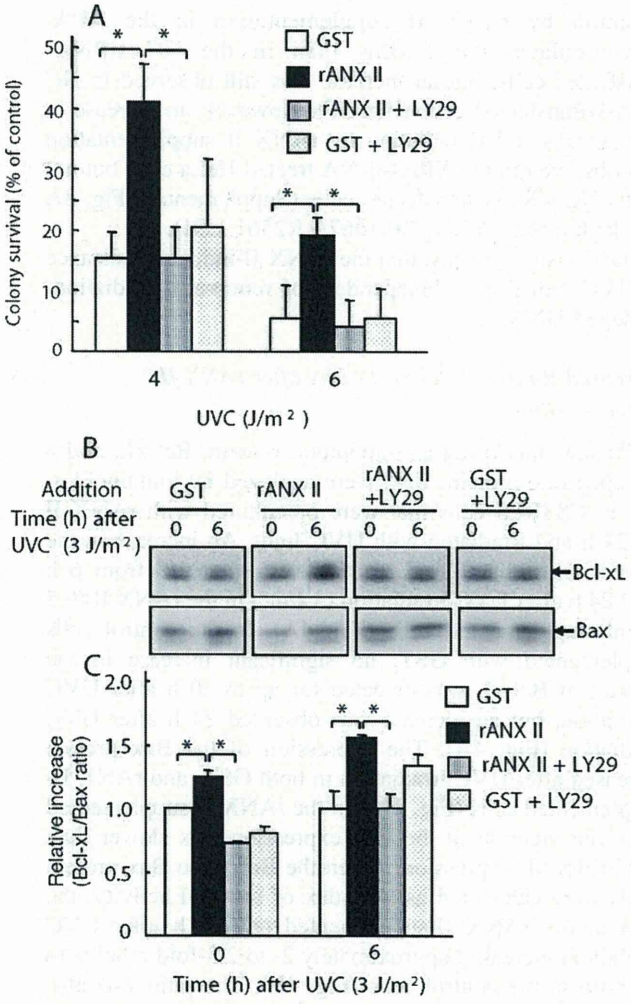

FIG. 5. Effects of the PI3K inhibitor on the rANX II supplementation-induced increase in the resistance to UVC radiation and Bcl-xL to Bax ratios. LY294002 (50 μM) (LY29) was added to the medium 30 min before addition of rANX II (0.5 μg/ml), and CS3BES cells were cultured in the presence of rANX II and LY29 for 24 h. After culturing, sensitivity to UVC-radiation-induced cell death at 4 J/m^2 and 6 J/m^2 was analyzed with the colony survival assay (panel A), and the expression levels of Bcl-xL and Bax proteins after UVC irradiation (3 J/m^2) were analyzed by immunoblotting (panel B), as described in the Materials and Methods. Bcl-xL and Bax protein levels were analyzed immediately (time 0) and 6 h after UVC irradiation, and the results are presented as the ratios of Bcl-xL to Bax (panel C). The ratios immediately (time 0) after UVC irradiation in the control cells (GST alone) are designated as 1. The data are presented as means ± SD. * indicates significant difference at $P < 0.05$ for rANX II addition compared to GST control or the combined addition of rANX with LY29004.

Control cells precultured with GST and LY29004 showed a slight but insignificant increase in survival activity after UVC irradiation relative to the control cells without LY29004 treatment (Fig. 5A).

In CS3BES cells treated with rANX II and LY29004, the expression levels of Bcl-xL and Bax were analyzed immediately (time 0) and 6 h after UVC irradiation because

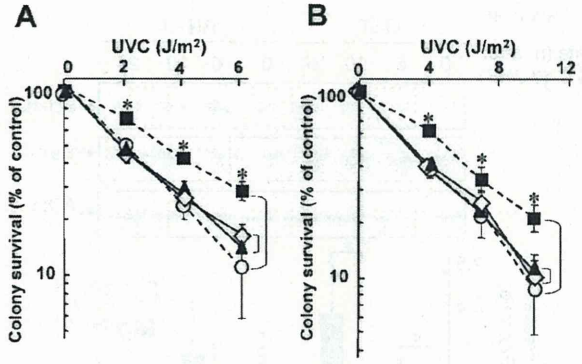

FIG. 6. Effect of Bcl-xL siRNA transfection on the rANX II supplementation-induced UVC-radiation resistance. CS3BES (panel A) and RSa (panel B) cells were transfected with 130 nM Bcl-xL siRNA (solid line) and NC siRNA (dotted line). Twenty-four hours after transfection, CS3BES and RSa cells were replated and cultured with rANX II (0.5 μg/ml) (■, ▲) and GST (0.017 μg/ml) (○, ◇) (panel A) or rANX II (1.0 μg/ml) (■, ▲) and GST (0.033 μg/ml) (○, ◇) (panel B) for 24 h, and sensitivity of the cells to UVC radiation was analyzed by the colony survival assay, as described in the Materials and Methods. The data are presented as means ± SD. * indicates significant difference at $P < 0.05$ for rANX II addition compared to GST control in the NC siRNA-transfected CE3BES and RSa cells.

the Bcl-xL to Bax ratios were significantly increased by rANX II supplementation at these times (Fig. 4B). LY29004 treatment suppressed the increased Bcl-xL to Bax ratios at both times (Fig. 5B and C). The control cells treated with LY29004 showed only a slight decrease in the Bcl-xL to Bax ratios at time 0 and an increase 6 h after UVC irradiation relative to cells that did not receive LY29004 treatment (Fig. 5C).

These results suggest that the increase in the Bcl-xL to Bax ratios is involved in the enhancement of UVC-radiation resistance by rANX II supplementation. Therefore, we examined the effect of siRNA transfection-induced Bcl-xL downregulation on the rANX II-induced UVC-radiation resistance in CS3BES and RSa cells. After being transfected with Bcl-xL siRNA, both cell types showed the decreased Bcl-xL levels and the decreased Bcl-xL to Bax ratios relative to the cells transfected with NC siRNA (Supplementary Fig. 5; http://dx.doi.org/10.1667/RR2561.1.S1); the ratios did not increase upon rANX II supplementation (data not shown). The rANX II supplementation-induced UVC-radiation resistance was not observed in either cell type upon downregulation of Bcl-xL, but resistance was observed in both cell types transfected with NC siRNA (Fig. 6).

DISCUSSION

We previously reported that the overproduction of human annexin II induced by cDNA transfection in human UVC-radiation-sensitive RSa cells confers an increased resistance to UVC-radiation-induced cell death (*6*). We are now

investigating the mechanisms underlying the annexin II-involved UVC-radiation resistance. Annexin II might play both intracellular and extracellular roles in UVC-radiation resistance. We examined the possible roles of extracellular annexin II in UVC-radiation resistance by using rANX II in human UVC-radiation-sensitive cells and found that the addition of extracellular rANX II in the culture medium resulted in an increased resistance to UVC-radiation-induced cell death in CS and RSa cells. Supplementation of rANX II was involved in the suppression of UVC-radiation-induced apoptosis in CS3BES cells [Supplementary Fig. 2 (http://dx.doi.org/10.1667/RR2561.1.S1) and Fig. 2D].

The time dependence of the UVC-radiation resistance-enhancing effect of rANX II addition was slow in CS3BES cells (Fig. 2A). Supplemented rANX II appeared to bind to the surface of the CS3BES cells 1 h after rANX II addition (Fig. 2E). The rapid binding, as reported in human endothelial cells (*27*), suggests that certain slow events, such as changes at the transcriptional and/or translational levels, are possibly required for rANX II to exert the UVC-radiation resistance-enhancing effect. The concentrations of rANX II used in the present study ranged from approximately 6 n*M* to 30 n*M*. Suppression of the rANX II supplementation-induced UVC-radiation resistance (Fig. 2C) and binding of annexin II to the cell surface (Fig. 2E) by EGTA suggests that the binding of rANX II is calcium-dependent. Additionally, detection of annexin II on the surface of the control cells (Fig. 2E) suggests the existence of endogenous annexin II on the surface of CS3BES cells. Human umbilical vein endothelial cells (HUVECs) can bind annexin II in a calcium-dependent manner, and these cells, when washed with EGTA, bound annexin II in a dose-dependent manner at concentrations of up to 60 n*M* and were apparently saturated at concentrations of over 80 n*M* (*27*). The saturable concentration curve of rANX II in CS3BES cells, even at low doses of rANX II (Fig. 2B), may be due to interference by endogenous annexin II expressed on the surface of the CS3BES cells. Alternatively, factors other than rANX II, including S100A10 (*18*), might also be required for the UVC-radiation resistance-enhancing effect in the cells.

It has been reported that treatment with extracellular interferon (*4*), a platelet-activating factor, and serotonin receptor antagonists (*28*) accelerated the repair of UV-radiation-damaged DNA. In contrast, the extracellular addition of rANX II did not change the removal of (6-4) photoproducts and cyclobutane pyrimidine dimers in CS3BES and RSa cells (Fig. 3B and C). It is possible that the NER process does not play a main role in the rANX II supplementation-associated UVC-radiation resistance in the cells. This possibility is also supported by the increased resistance to UVC radiation in the rANX II-supplemented XP cells (Fig. 3D and E), which are deficient in NER, and in the XPA-downregulated AP^r-1 and HeLa cells (Fig. 3F and Supplementary Fig. 3B; http://dx.doi.org/10.1667/RR2561.1.S1). However, we cannot rule out the possibility that other repair pathways, for example translesion synthesis (TLS) (*29*), might play roles in the rANX II supplementation-associated UVC-radiation resistance.

In rANX II-supplemented CS3BES, RSa and AP^r-1 cells, the Bcl-xL to Bax expression ratios increased before and after UVC irradiation relative to the ratios in the respective control cells (Fig. 4 and Supplementary Fig. 4; http://dx.doi.org/10.1667/RR2561.1.S1). Bcl-xL is an anti-apoptotic protein, and Bax is a pro-apoptotic protein (*30*). The relative expression ratios of pro-apoptotic proteins to anti-apoptotic proteins have been reported to correlate with cellular sensitivity to the lethal effects of anti-cancer drugs (*23*). Intimate relationships have been reported between increased Bcl-xL expression levels and resistance to pro-apoptotic stimuli, such as anti-cancer drugs, hypoxia and matrix detachment (*31*, *32*). Therefore, the increase in the Bcl-xL to Bax ratios found here may be related to the increased resistance to UVC-radiation-induced cell death in the rANX II-supplemented cells. In fact, the downregulation of Bcl-xL by siRNA transfection in CS3BES and RSa cells suppressed the increased UVC-radiation resistance by rANX II supplementation (Fig. 6). To our knowledge, this is the first report that the ratio of Bcl-xL to Bax is possibly increased by extracellular annexin II, thus leading to UVC-radiation resistance. The rANX II-induced change in the Bcl-xL/Bax ratios after UVC irradiation seemed to differ with the three cell types. In the UV-radiation-sensitive cells, CS3BES and RSa, the ratios peaked at 6 h after UVC irradiation but the increased ratios did not continue 6 h later, while in the UVC-radiation-resistant AP^r-1 cells, the rANX II-induced increase in the Bcl-xL/Bax ratios continued until 24 h. The difference might be related to the different sensitivity to UVC radiation; nevertheless, the details of the molecular mechanisms by which the ratios increase remain unclear.

In AP^r-1 cells, the Bcl-xL to Bax ratios increased greatly after UVC irradiation, even without the addition of rANX II, and the UVC-radiation resistance-increasing effect of rANX II was weak [Supplementary Fig. 4C and D (http://dx.doi.org/10.1667/RR2561.1.S1) and Fig. 3F]. In HeLa cells, a similar increase in the Bcl-xL to Bax ratios was not observed. The supplementation of rANX II did not increase the growth activity of cells that did not receive UVC radiation in any of the cell types studied here. Thus rANX II might confer a survival advantage after UVC irradiation in UVC-radiation-sensitive cells in which the surviving activity may be intrinsically weak. However, there is the possibility that the UVC-radiation resistance-increasing effect of rANX II, without an increase in NER activity, might lead to the induction of mutations; nevertheless, our preliminary experiments suggest that the frequency of UVC-radiation-induced mutation was not increased by rANX II supplementation in RSa cells (data not shown). Other repair pathways might function in the rANX II-supplemented cells.

Treatment with LY29004, a PI3K inhibitor, suppressed not only the enhancement of resistance to UVC radiation but also the increase in the Bcl-xL to Bax expression ratios by rANX II supplementation (Fig. 5A–C). The levels of phospho-Akt actually increased in the rANX II-supplemented cells relative to the phospho-Akt levels in the control cells, and this increase was suppressed by LY29004 (Supplementary Fig. 6; http://dx.doi.org/10.1667/RR2561.1.S1). Therefore, a PI3K/Akt-dependent pathway may be involved in the increase of the Bcl-xL to Bax ratios and the UVC-radiation resistance by rANX II supplementation. Annexin II is known to function as a cell surface receptor for ligands, including progastrin (PG) and gastrin peptides (*16*) and cathepsin B (*17*). Moreover, annexin II is thought to mediate the anti-apoptotic effect of PG in pancreatic cancer (*33*) and the urokinase type of plasminogen activator (uPA) signaling through interaction with cathepsin B (*17*). PG and uPA signaling that leads to protection against cell death has been shown to be mediated by PI3K-dependent pathways (*33, 34*). Furthermore, uPA elicits an enhancement of PI3K and MAPK activities and enhances the transcriptional activation of Bcl-xL expression (*34*). Based on these previous reports, the data shown here suggest that these ligands for annexin II might play roles in UVC-radiation resistance.

It is known that annexin II can be secreted into the extracellular compartment from human cells, such as HUVECs, that have received a temperature stress (*35*) or mouse epidermal cells that were exposed to low doses of radiation (*18*). In the latter cells, secreted annexin II was reported to be involved in the resistance to apoptosis; however, the molecular mechanisms underlying the secretion of annexin II are not well known. Therefore, a search for environmental compounds or bioactive substances that increase the extracellular release of annexin II and elucidating the mechanisms of annexin II release would supply useful information for reducing UV-radiation hypersensitivity in CS patients. A search for peptides that mimic extracellular annexin II is also important for reducing UV-radiation sensitivity.

ACKNOWLEDGMENTS

We thank Dr. M. Zahed for technical support and R. Nobuhara for technical assistance. This work was supported in part by grants-in-aid from the following organizations: the Smoking Research Foundation, the Tokyu Foundation for a Better Environment, the Tsuchiya Foundation, the Goho Life Science International Foundation, the Kieikai Research Foundation, the Ministry of Health, Labor and Welfare for the Intractable Diseases Treatment Research Program and the Japan Society for the Promotion of Science (Japan).

Received: January 7, 2011; accepted September 7, 2011; published online: October 4, 2011

REFERENCES

1. Sugarman GI, Landing BH, Reed WB. Cockayne syndrome: clinical study of two patients and neuropathologic findings in one. Clin Pediatr 1977; 16:225–32.
2. Schmickel RD, Chu EH, Trosko JE, Chang CC. Cockayne syndrome: a cellular sensitivity to ultraviolet light. Pediatrics 1977; 60:135–9.
3. Mayne LV, Lehmann AR. Failure of RNA synthesis to recover after UV irradiation: an early defect in cells from individuals with Cockayne's syndrome and xeroderma pigmentosum. Cancer Res 1982; 42:1473–8.
4. Suzuki N, Suzuki H, Kojima T, Sugita K, Takakubo Y, Okamoto S. Effects of human interferon on cellular response to UV-sensitive human cell strains. Mutat Res 1988; 198:207–14.
5. Wano C, Kita K, Takahashi S, Sugaya S, Hino M, Hosoya H, et al. Protective role of HSP27 against UVC-induced cell death in human cells. Exp Cell Res 2004; 298:584–92.
6. Jin YH, Kita K, Sun Z, Tong XB, Nie H, Suzuki N. The roles of HSP27 and annexin II in resistance to UVC-induced cell death: comparative studies of the human UVC-sensitive and -resistant cell lines RSa and AP^r-1. Biosci Biotechnol Biochem 2009; 73:1318–22.
7. Tong XB, Kita K, Karata K, Zhu CL, Sugaya S, Ichimura Y, et al. Annexin II, a novel HSP27-interacted protein, is involved in resistance to UVC-induced cell death in human AP^r-1 cells. Photochem Photobiol 2008; 84:1455–61.
8. Benz J, Hofmann A. Annexins: from structure to function. Biol Chem 1997; 378:177–83.
9. Creutz CE. The annexins and exocytosis. Science 1992; 258:924–31.
10. Emans N, Gorvel JP, Walter C, Gerke V, Kellner R, Griffiths G, et al. Annexin II is a major component of fusogenic endosomal vesicles. J Cell Biol 1993; 120:1357–69.
11. Siever DA, Erickson HP. Extracellular annexin II. Int J Biochem Cell Biol 1997; 29:1219–23.
12. Hajjar KA, Jacovina AT, Chacko J. An endothelial cell receptor for plasminogen/tissue plasminogen activator. I. Identity with annexin II. J Biol Chem 1994; 269:21191–7.
13. Singh P. Role of Annexin II in GI cancers: interaction with gastrins/progastrins. Cancer Lett 2007; 252:19–35.
14. Chung CY, Murphy-Ullrich JE, Erickson HP. Mitogenesis, cell migration, and loss of focal adhesions induced by tenascin-C interacting with its cell surface receptor, annexin II. Mol Biol Cell 1996; 7:883–92.
15. Esposito I, Penzel R, Chaib-Harrireche M, Barcena U, Bergmann F, Riedl S, et al. Tenascin C and annexin II expression in the process of pancreatic carcinogenesis. J Pathol 2006; 208:673–85.
16. Singh P, Wu H, Clark C, Owlia A. Annexin II binds progastrin and gastrin-like peptides, and mediates growth factor effects of autocrine and exogenous gastrins on colon cancer and intestinal epithelial cells. Oncogene 2007; 26:425–40.
17. Mai J, Finley RL Jr, Waisman DM, Sloane BF. Human procathepsin B interacts with the annexin II tetramer on the surface of tumor cells. J Biol Chem 2000; 275:12806–12.
18. Weber TJ, Opresko LK, Waisman DM, Newton GJ, Quesenberry RD, Bollinger N, et al. Regulation of the low-dose radiation paracrine-specific anchorage-independent growth response by annexin A2. Radiat Res 2009; 172:96–105.
19. Lehmann AR, Thompson AF, Harcourt SA, Stefanini M, Norris PG. Cockayne's syndrome: correlation of clinical features with cellular sensitivity of RNA synthesis to UV irradiation. J Med Genet 1993; 30:679–82.
20. Mayne LV, Priestley A, James MR, Burke JF. Efficient immortalization and morphological transformation of human fibroblasts by transfection with SV40 DNA linked to a dominant marker. Exp Cell Res 1986; 162:530–8.
21. Kuwata T, Oda T, Sekiya S, Morinaga N. Characteristics of a human cell line successively transformed by Rous sarcoma virus and Simian virus 40. J Natl Cancer Inst 1976; 56:919–26.
22. Isogai E, Ishijima S, Sonoda T, Kita K, Suzuki H, Hasegawa R, et

al. Protease activation following UV irradiation is linked to hypomutability in human cells selected for resistance to combination of UV and antipain. Mutat Res 1998; 403:215–22.

23. Done M, Chen SP, Kita K, Ichimura Y, Guo WZ, Lu S, et al. Antiproliferative and apoptosis-inducible activity of Sarcodonin G from Sarcodon scabrosus in HeLa cells. Int J Oncol 2009; 34: 201–7.
24. Sugita K, Suzuki N, Kojima T, Tanabe Y, Nakajima H, Hayashi A, et al. Cockayne syndrome with delayed recovery of RNA synthesis after ultraviolet irradiation but normal ultraviolet survival. Pediatr Res 1987; 21:34–7.
25. Hirano J, Wang X, Kita K, Higuchi Y, Nakanishi H, Uzawa K, et al. Low levels of NPM gene expression in UV-sensitive human cell lines. Cancer Lett 2000; 153:183–8.
26. Gorza L, Vitadello M. Reduced amount of the glucose-regulated protein GRP94 in skeletal myoblasts results in loss of fusion competence. FASEB J 2000; 14:461–75.
27. Hajjar KA, Guevara CA, Lev E, Dowling K, Chacko J. Interaction of the fibrinolytic receptor, annexin II, with the endothelial cell surface. Essential role of endonexin repeat 2. J Biol Chem 1996; 271:21652–9.
28. Sreevidya CS, Fukunaga A, Khaskhely NM, Masaki T, Ono R, Nishigori C, et al. Agents that reverse UV-induced immune suppression and photocarcinogenesis affect DNA repair. J Invest Dermatol 2010; 130:1428–37.
29. McGregor WG, Wei D, Maher VM, McCormick JJ. Abnormal, error-prone bypass of photoproducts by xeroderma pigmentosum variant cell extracts results in extreme strand bias for the kinds of mutations induced by UV light. Mol Cell Biol 1999; 19:147–54.
30. Green DR, Kroemer G. The pathophysiology of mitochondrial cell death. Science 2004; 305:626–9.
31. Wang X, Zhou Y, Kim HP, Song R, Zamegar R, Ryter SW, et al. Hepatocyte growth factor protects against hypoxia/reoxygenation-induced apoptosis in endothelial cells. J Biol Chem 2004; 279:5237–43.
32. Coll ML, Rosen K, Ladeda V, Filmus J. Increased Bcl-xL expression mediates V-Src-induced resistance to anoikis in intestinal epithelial cells. Oncogene 2002; 21:2908–13.
33. Rengifo-Cam W, Umar S, Sarkar S, Singh P. Antiapoptotic effects of progastrin on pancreatic cancer cells are mediated by sustained activation of nuclear factor-kappaB. Cancer Res 2007; 67:7266–74.
34. Alfano D, Iaccarino I, Stoppelli MP. Urokinase signaling through its receptor protects against anoikis by increasing BCL-xL expression levels. J Biol Chem 2006; 281:17758–67.
35. Deora AB, Kreitzer G, Jacovina AT, Hajjer KA. An annexin 2 phosphorylation switch mediates p11-dependent translocation of annexin 2 to the cell surface. J Biol Chem 2004; 279:43411–8.

CLINICAL GENETICS
An International Journal of Genetics, Molecular, and Personalized Medicine

Clin Genet 2011: 79: 196–198
Printed in Singapore. All rights reserved

CLINICAL GENETICS
doi: 10.1111/j.1399-0004.2010.01527.x

Letter to the Editor

Entire *PTCH1* deletion is a common event in point mutation-negative cases with nevoid basal cell carcinoma syndrome in Japan

To the Editor:

Nevoid basal cell carcinoma syndrome [NBCCS (OMIM 109400)], also called Gorlin syndrome, is an autosomal dominant neurocutaneous disorder characterized by large body size, developmental and skeletal abnormalities, sensitivity to radiation, and an increased incidence of cancers such as basal cell carcinoma (BCC) and medulloblastoma (1). NBCCS is caused by inactivating mutations in the *Patched-1* (*PTCH1*) gene (2, 3). Heterozygous loss of *PTCH1* found in certain sporadic and familial cases of BCC indicates that *PTCH1* is also a tumor suppressor gene (4, 5).

Despite extensive efforts to detect mutations, they are still unidentified in 25–60% of patients (6–8). To date, we have analyzed 38 patients with NBCCS from 32 families. Eight of the families did not harbor any *PTCH1* mutations detectable by polymerase chain reaction (PCR)-based direct sequencing of the exons. To investigate the possibility of large deletions involving the *PTCH1* gene, we employed a high-resolution array-based comparative genomic hybridization technology. Consequently, we identified genomic deletions involving *PTCH1* in seven individuals from five of the eight point mutation-negative families (Fig. S1). These patients are listed in Table 1. Some of them have been reported previously by us (9) and one patient reported by others (NS6) (10) is also included in the table, all of which are of Japanese origin. To our knowledge, this table includes all the patients with *PTCH1* deletions in which the breakpoints have been identified at the nucleotide level. A schematic representation of each deletion's size together with the deleted genes is shown in Fig. 1a. Unlike in cases of Sotos syndrome and neurofibromatosis type 1, no recurrent breakpoints were observed in these patients (11, 12). Whereas deletions larger than 2.4 Mb were generated by non-homologous end joining, smaller ones (less than 1.2 Mb) were produced by *Alu*-mediated nonallelic homologous recombination (Fig. S2).

G19 and G36 inherited the deletion from their mothers (G27 and G43, respectively), whereas the deletion in NS6 is of paternal origin. The breakpoint sequences in these cases were completely conserved through generations. Other patients (G35, G10 and G5) did not have a family history of NBCCS and, therefore, the deletions seemed to be *de novo*. Patients harboring deletions of less than 2.4 Mb did not exhibit any phenotypes atypical for NBCCS despite that up to 22 RefSeq genes (four disease genes) were included in the deleted region. This implies that hemizygous loss of these genes, except for *PTCH1*, might not have an influence on any observable phenotypes. In contrast, deletions larger than 5.3 Mb led to phenotypes unusual for NBCCS including severe mental and motor retardation, epilepsy, and hypotonia (Table 1).

Interestingly, each *Alu*-mediated deletion was mediated by a distinct path of rearrangement (Fig. 1b). G36/43 had a crossing over point within the *Alu* elements generating a hybrid *Alu* element. In G19/27, however, the crossing over occurred near the poly-A tail of the proximal *Alu* element (9). Therefore, the proximal *Alu* remained intact while the distal *Alu* was deleted. In the third case, NS6, crossing over occurred at the 5′ end of the *Alu* elements and removed both *Alu* sequences leaving two short direct repeats flanking an *Alu* element on both sides called target-site duplications (10).

To date, we have analyzed 32 NBCCS families and identified entire deletions of *PTCH1* in 5 families. This implies that 16% of NBCCS families (five of the eight point mutation-negative families) can be explained by the entire loss of *PTCH1*. Mutations are not observed in the *PTCH1*-coding sequences in considerable numbers of NBCCS cases not only in Japanese but also in other ethnicities and, apart from *PTCH1*, only one *PTCH2* and one *SUFU* mutation in NBCCS have been

Table 1. NBCCS patients with gene deletions

Patient No.	Age (years)	Size	Deleted nucleotide No.[a]	Deleted RefSeq genes[b]	Deleted disease genes[b]	Predicted mechanism of deletion	Atypical phenotypes
G19[c]	10	165 kb	97,187,146–197,350,058	1	1	Alu-mediated NAHR[d]	None
G27[e]	40	165 kb	97,187,146–97,350,058	1	1	Alu-mediated NAHR	None
G36	8 M[f]	1.1 Mb	96,766,985–97,885,391	9	2	Alu-mediated NAHR	None
G43[g]	32	1.1 Mb	96,766,985–97,885,391	9	2	Alu-mediated NAHR	None
NS6[h]	NA[i]	1.2 Mb	96,070,054–97,646,323[j]	13	3	Alu-mediated NAHR	None
G35	5	2.4 Mb	95,880,121–98,238,462	22	4	NHEJ[k] with 2-bp overlap	None
G10[c]	8	5.3 Mb	94,898,311–100,101,915	58	6	NHEJ with 1-bp overlap	severe mental and motor retardation, epilepsy, hypotonia, inguinal hernia
G5[c]	12	11 Mb	90,617,332–101,647,101	93	13	NHEJ with 7-bp addition	severe mental and motor retardation, epilepsy, hypotonia, webbed neck, hydronephrosis

[a]Nucleotide numbers are based on UCSC Genome Browser on Human March 2006 Assembly (hg18).
[b]Numbers of the deleted genes are based on Database of Genomic variants (http://projects.tcag.ca/variation/).
[c]Fujii et al. 2007 (9).
[d]nonallelic homologous recombination.
[e]G19's mother.
[f]8 months.
[g]G36's mother.
[h]Takahashi et al. 2009 (10).
[i]Not available.
[j]Distal breakpoint is ambiguous due to the complicated structure of the deletion (10).
[k]non-homologous end joining.

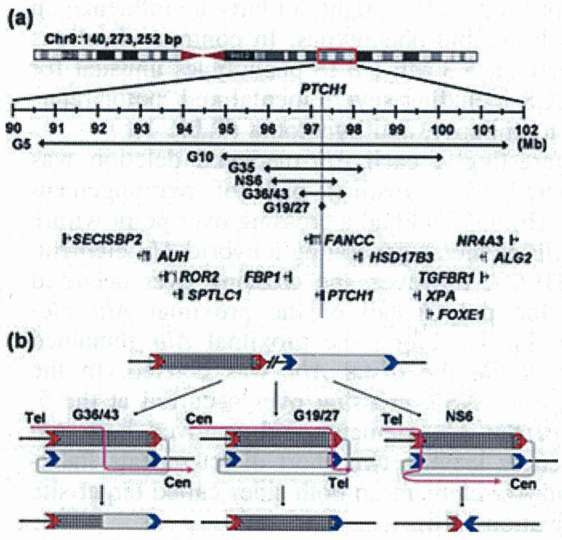

Fig. 1. Schematic representation of the deletions. (**a**) Architecture of the deleted region. Horizontal arrows represent the deleted regions in the six families listed in Table 1. Disease genes are depicted at the bottom. Vertical dotted lines indicate the positions of *PTCH1*. (**b**) Three different types of recombination between *Alu* elements observed in NBCCS patients. Black and gray lines represent flanking and intervening regions, respectively. Curved red arrows show the paths of recombination events. Red and blue arrowheads represent target-site duplications (TSDs) of the two elements, respectively. Cen, centromeric; Tel, telomeric.

reported (13, 14). Therefore, it is strongly advisable to investigate the possibility of the gene deletion in point mutation-negative cases.

Supporting Information

The following Supporting information is available for this article:

Fig. S1. Microarray profile of two individuals with a copy number loss at 9q22. Probes are ordered on the x-axis according to physical mapping positions. Test over reference signal intensity ratios for each probe are given on the y axis. For clarity, data are smoothed over a 50-probe window. The position of *PTCH1* is indicated by a vertical dotted line. Disease genes lying in this region are schematically indicated at the bottom.

Fig. S2. DNA sequence of junction fragments. The DNA sequence for each deletion-specific junction fragment obtained by polymerase chain reaction (PCR) was aligned to the wild-type flanking genome sequence for both proximal and distal breakpoints. Alignments with the proximal boundary are shaded in light gray, and those with the distal boundary in dark gray. The estimated cross over points are shaded in red. (A) Sequence alignment in G36/43. Red lines surround *Alu* sequences. The precise length of polyT could not be determined due to the heterogeneity of the PCR product (A_{20-22}). (B) Sequence alignment in G35.

Additional Supporting information may be found in the online version of this article.

Please note: Wiley-Blackwell Publishing is not responsible for the content or functionality of any supplementary materials supplied by the authors. Any queries (other than missing material) should be directed to the corresponding author for the article.

Letter to the Editor

Acknowledgements

We thank all patients, their families and collaborating doctors for participating in this study. We are also grateful to Noriko Ito for technical support. This work was partly supported by a Grant-in-Aid for Research on Intractable Diseases from the Ministry of Health, Labor and Welfare, Japan (No. H22-120), and by a Grant-in-Aid for Scientific Research (C) from the Ministry of Education, Culture, Sports, Science and Technology, Japan (No. 21591313).

K Nagao[a]
K Fujii[b]
K Saito[c]
K Sugita[d]
M Endo[b]
T Motojima[e]
H Hatsuse[a]
T Miyashita[a]

[a]Department of Molecular Genetics, Kitasato University School of Medicine, Sagamihara, Japan,
[b]Department of Pediatrics, Chiba University Graduate School of Medicine, Chiba, Japan,
[c]Institute of Medical Genetics, Tokyo Women's Medical University, Tokyo, Japan,
[d]Division of Child Health, Faculty of Education, Chiba University, Chiba, Japan, and
[e]Department of Pediatrics, Motojima General Hospital, Ota, Japan

References

1. Gorlin RJ. Nevoid basal-cell carcinoma syndrome. Medicine (Baltimore) 1987: 66: 98–113.
2. Johnson RL, Rothman AL, Xie J et al. Human homolog of *patched*, a candidate gene for the basal cell nevus syndrome. Science 1996: 272: 1668–1671.
3. Hahn H, Wicking C, Zaphiropoulous PG et al. Mutations of the human homolog of Drosophila *patched* in the nevoid basal cell carcinoma syndrome. Cell 1996: 85: 841–851.
4. Gailani MR, Stahle-Backdahl M, Leffell DJ et al. The role of the human homologue of *Drosophila patched* in sporadic basal cell carcinomas. Nat Genet 1996: 14: 78–81.
5. Unden AB, Holmberg E, Lundh-Rozell B et al. Mutations in the human homologue of *Drosophila patched* (*PTCH*) in basal cell carcinomas and the Gorlin syndrome: different *in vivo* mechanisms of *PTCH* inactivation. Cancer Res 1996: 56: 4562–4565.
6. Fujii K, Kohno Y, Sugita K et al. Mutations in the human homologue of *Drosophila patched* in Japanese nevoid basal cell carcinoma syndrome patients. Hum Mutat 2003: 21: 451–452.
7. Marsh A, Wicking C, Wainwright B, Chenevix-Trench G. DHPLC analysis of patients with Nevoid Basal Cell Carcinoma Syndrome reveals novel *PTCH* missense mutations in the sterol-sensing domain. Hum Mutat 2005: 26: 283.
8. Lindström E, Shimokawa T, Toftgård R, Zaphiropoulos PG. PTCH mutations: distribution and analyses. Hum Mutat 2006: 27: 215–219.
9. Fujii K, Ishikawa S, Uchikawa H et al. High-density oligonucleotide array with sub-kilobase resolution reveals breakpoint information of submicroscopic deletions in nevoid basal cell carcinoma syndrome. Hum Genet 2007: 122: 459–466.
10. Takahashi C, Kanazawa N, Yoshikawa Y et al. Germline *PTCH1* mutations in Japanese basal cell nevus syndrome patients. J Hum Genet 2009: 54: 403–408.
11. Kurotaki N, Harada N, Shimokawa O et al. Fifty microdeletions among 112 cases of Sotos syndrome: low copy repeats possibly mediate the common deletion. Hum Mutat 2003: 22: 378–387.
12. Dorschner MO, Sybert VP, Weaver M, Pletcher BA, Stephens K. *NF1* microdeletion breakpoints are clustered at flanking repetitive sequences. Hum Mol Genet 2000: 9: 35–46.
13. Fan Z, Li J, Du J et al. A missense mutation in *PTCH2* underlies dominantly inherited NBCCS in a Chinese family. J Med Genet 2008: 45: 303–308.
14. Pastorino L, Ghiorzo P, Nasti S et al. Identification of a *SUFU* germline mutation in a family with Gorlin syndrome. Am J Med Genet A 2009: 149A: 1539–1543.

Correspondence:
Toshiyuki Miyashita, MD, PhD
Department of Molecular Genetics
Graduate School of Medical Science
Kitasato University
1-15-1 Kitasato
Minami-ku
Sagamihara 252-0374
Japan
Tel.: +81 42 778 8816
Fax: +81 42 778 9214
e-mail: tmiyashi@med.kitasato-u.ac.jp

Multiple keratocystic odontogenic tumors associated with nevoid basal cell carcinoma syndrome having distinct *PTCH1* mutations: a case report

Ryo Sasaki, DDS, PhD,[a] Toshiyuki Miyashita, MD, PhD,[b] Naoyuki Matsumoto, DDS, PhD,[c] Katsunori Fujii, MD, PhD,[d] Kayoko Saito, MD, PhD,[e] and Tomohiro Ando, DDS, PhD,[f]
Tokyo, Kahagawa, and Chiba, Japan
TOKYO WOMEN'S MEDICAL UNIVERSITY SCHOOL OF MEDICINE, KITASATO UNIVERSITY SCHOOL OF MEDICINE, NIHON UNIVERSITY SCHOOL OF DENTISTRY, AND CHIBA UNIVERSITY GRADUATE SCHOOL OF MEDICINE

Nevoid basal cell carcinoma syndrome (NBCCS) is a rare autosomal dominant disorder characterized by developmental abnormalities and a predisposition to cancers. Although multiple jaw tumors, such as keratocystic odontogenic tumors (KCOTs), are one of the most frequent complications in NBCCS, the molecular mechanism for how KCOTs develop in NBCCS is poorly understood. A 15-year-old girl with 2 jaw tumors was diagnosed as NBCCS according to the clinical criteria. The pathologic findings indicated that the 2 tumors were consistent with KCOTs. A *PTCH1* mutation, c.1472delT, was detected in her peripheral blood as well as in the 2 tumors. Interestingly, an additional *PTCH1* mutation, c.264_265insAATA, that was not present in the peripheral blood, was found in the maxillary tumor but not the mandibular tumor. The Ki-67 labeling index was significantly higher in the maxillary KCOT (17.7%) than in the mandibular KCOT (14.3%). These findings indicate distinct molecular mechanisms of tumorigenesis in these KCOTs. **(Oral Surg Oral Med Oral Pathol Oral Radiol Endod 2010;110: e41-e46)**

Nevoid basal cell carcinoma syndrome (NBCCS), or Gorlin syndrome, is an autosomal dominant disorder that was first described by Gorlin and Goltz in 1960.[1] It is characterized by developmental abnormalities such as bifid ribs and cleft lip and palate. It is also characterized by a high incidence of tumorigenesis, such as basal cell carcinoma and medulloblastoma. Palmar and plantar pits and calcification of the falx cerebri are also included as pathognomonic signs of NBCCS.[1-5] Its prevalences are estimated to range from 1 in 56,000 in the United Kingdom to 1 in 164,000 in Australia.[2,4] However, the prevalences remain unreported in other countries, including Japan.

The human homolog of *Drosophila patched*, *PTCH1*, which is mapped to the NBCCS locus on chromosome 9q22.3, was first reported to contain mutations in NBCCS patients in 1996.[6,7] Subsequently, 75% of Japanese NBCCS patients were found to have *PTCH* mutations.[8] Because the PTCH1 protein functions as a suppressive receptor for the secretory protein sonic hedgehog (SHH), the phenotypes of NBCCS are believed to develop based on constitutive activation of the SHH pathway.[9]

Multiple jaw cysts, which are currently termed keratocystic odontogenic tumors (KCOTs), can be the first signs of NBCCS.[10] The incidence of KCOTs in NBCCS ranges from 75% to 90%.[2-5] KCOTs, which were previously known as odontogenic keratocysts, are benign cystic lesions, but they often show locally destructive behaviors and high recurrence rates.[11] Therefore, KCOTs are defined as benign neoplasms of odontogenic origin in the World Health Organization classification revised in 2005.[12] However, the molecular mechanism for how KCOTs develop in NBCCS patients is poorly understood.

Supported in part by a Grant-in Aid for Research on Intractable Diseases from the Ministry of Health, Labor, and Welfare, Japan (no. H21-058), and by a Grant-in-Aid for Scientific Research from the Ministry of Education, Culture, Sports, Science, and Technology, Japan (no. 21591313).
[a]Assistant Professor, Department of Oral and Maxillofacial Surgery and Institute of Advanced Biomedical Engineering and Science, Tokyo Women's Medical University School of Medicine.
[b]Professor, Department of Molecular Genetics, Kitasato University School of Medicine.
[c]Assistant Professor, Department of Pathology, Nihon University School of Dentistry.
[d]Assistant Professor, Department of Pediatrics, Chiba University Graduate School of Medicine.
[e]Professor, Institute of Medical Genetics, Tokyo Women's Medical University School of Medicine.
[f]Professor, Department of Oral and Maxillofacial Surgery, Tokyo Women's Medical University School of Medicine.
Received for publication Feb 19, 2010; returned for revision Apr 1, 2010; accepted for publication Apr 5, 2010.
1079-2104/$ - see front matter

doi:10.1016/j.tripleo.2010.04.006

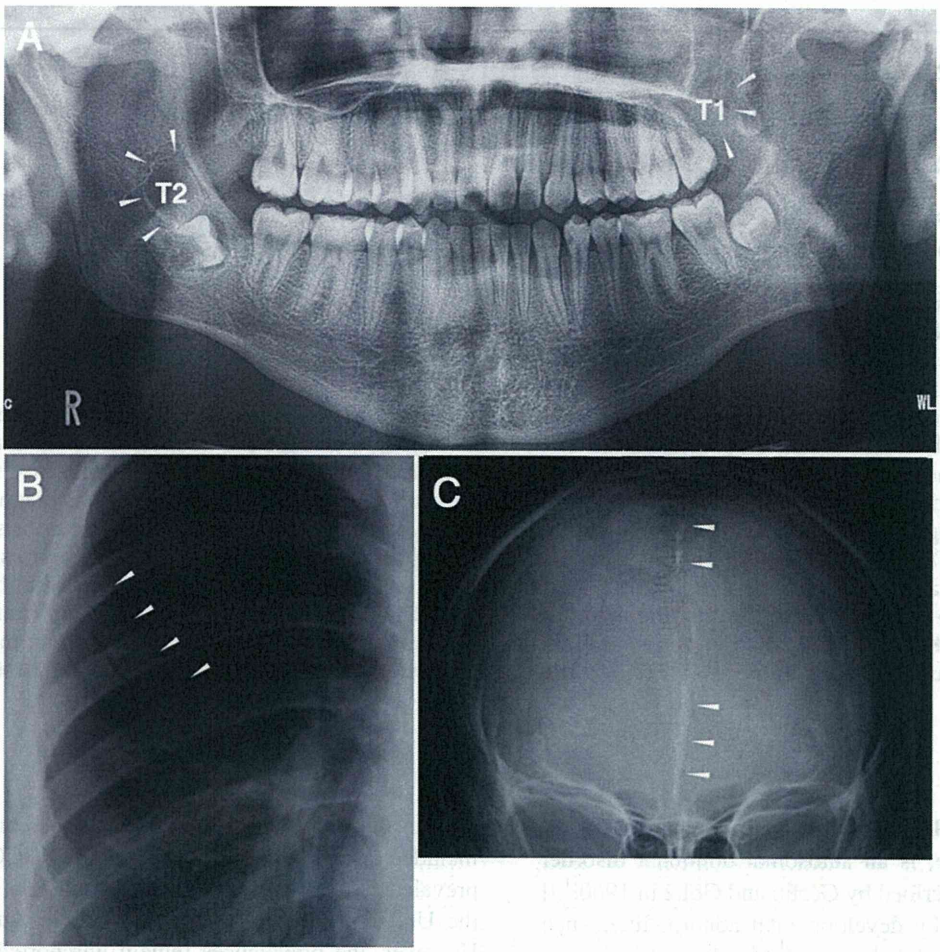

Fig. 1. X-ray images of the patient. **A,** Two jaw cysts (*arrowheads*) were detected in the maxilla (T1) and mandible (T2) in a panoramic x-ray image. **B and C,** Bifid ribs (*B*) and calcification of the falx cerebri (*C*) were also observed (*arrowheads*).

In the present study, we carried out a genetic analysis of the *PTCH1* gene to confirm the clinical diagnosis of NBCCS in a 15-year-old female patient. We also analyzed the *PTCH1* mutations in her KCOT tissues. As a result, an additional mutation was found in the maxillary KCOT but not in the mandibular KCOT. To investigate the effects of the presence or absence of this somatic mutation, we analyzed the expressions of prognostic molecular markers for KCOTs,[13-16] including Ki-67, cyclin D1, and p53, by immunohistochemistry.

CASE REPORT

A 15-year-old female patient was referred to our Department of Oral and Maxillofacial Surgery for 2 jaw cysts in the maxillary and mandibular regions, which were detected in a panoramic x-ray image taken by a local dental clinic (Fig. 1, *A*) that she attended because of pus discharge from the left maxillary gingiva. At 8 years of age, she had undergone a fenestration operation for a follicular cyst of the right mandibular cuspid in our department. After the operation, a panoramic x-ray image had shown no maxillary or mandibular cysts. She had no family history of NBCCS. She exhibited palmar pits, calcification of the falx cerebri, and bridging of the sella and bifid ribs (Fig. 1, *B* and *C*) and was clinically diagnosed with NBCCS according to the clinical criteria of Kimonis et al.[3] (Table I). Magnetic resonance imaging of the brain showed no evidence of medulloblastoma. She underwent 2 jaw cyst removals under general anesthesia. The pathologic findings of the maxillary and mandibular cysts indicated KCOTs. Genetic counseling and genetic testing were undertaken at the Institute of Medical Genetics, Tokyo Women's Medical University and Kitasato University. She had no tumor recurrences for >18 months after the surgery.

Mutational analysis

The study described below was approved by the Ethics Committee at Tokyo Women's Medical University and Kitasato University. After written informed consent was obtained, peripheral blood and tumor tissue samples were taken from

Table I. Clinical characteristics of the 15-year-old female patient according to the diagnostic criteria by Kimonis et al.[3]

Major Criteria	
>2 BCCs, or 1 BCC if <20 y	No
Odontogenic keratocysts of the jaw proven by histology	Yes
≥3 palmar or plantar pits	Yes
Bilamellar calcification of the falx cerebri	Yes
Bifid, fused, or markedly splayed ribs	Yes
First-degree relative with NBCCS	No
Minor Criteria	
Macrocephaly determined after adjustment for height	No
Congenital malformations	No
Other skeletal abnormalities	No
Radiologic abnormalities	Bridging of the sella turcica
Ovarian fibroma	No
Medulloblastoma	No

BCC, Basal cell carcinoma; *NBCCS,* nevoid basal cell carcinoma syndrome.

the patient. Genomic DNA was extracted using a QIAamp DNA Blood Midi Kit (Qiagen, Hilden, Germany). The genomic DNA samples were amplified with primers for all exons of the *PTCH1* gene as described previously.[8,10] The amplified products were gel-purified using a QIAex II Gel Extraction Kit (Qiagen) and cycle-sequenced with a BigDye Terminator v3.1 Cycle Sequencing Kit (Applied Biosystems, Foster City, CA) in both directions. The sequences were analyzed using a 3130 Genetic Analyzer (Applied Biosystems).

Immunohistochemistry

The KCOTs in the maxilla and mandible were compared for their expressions of prognostic factors for KCOTs, including Ki-67, cyclin D1, and p53.[13-16] Immunohistochemistry was performed on 10% neutral-buffered formalin-fixed and paraffin-embedded tissue sections. The tissue sections were deparaffinized in xylene and subjected to antigen retrieval by autoclaving (121°C, 2 atm, 15 min) in 0.01 mol/L citrate buffer (pH 6.0). After treatment with 3% hydrogen peroxide and a protein-blocking reagent (Dako, Glostrup, Denmark), the sections were incubated with primary antibodies against Ki-67 (clone MIB-1, 1:400 dilution; Dako), cyclin D1 (clone SP4, 1:250 dilution; Nichirei Bioscience, Tokyo, Japan), and p53 (clone DO-7, 1:300 dilution; Dako) at 4°C overnight. The sections were then incubated with a Dako Envision Kit (Dako), and antibody-antigen complexes were visualized by 3,3̀-diaminobenzidine staining. The sections were counterstained with Mayer hematoxylin and examined using a Leica DFC-6000B microscope system equipped with an ×40 objective lens (Leica Microsystems, Wetzlar, Germany). Digital images were captured with a CCD camera (DFC500; Leica Microsystems) and the numbers of Ki-67–, cyclin D1–, and p53-positive cells were counted in 5 randomly selected fields. The results were expressed as labeling indices (LI) for Ki-67, cyclin D1, and p53 as percentages of positive cells in the whole epithelial layer. The data are presented as mean ± SD. The significance of differences in the Ki-67, cyclin D1, and p53 LIs between the maxillary and mandibular tumors were analyzed by the Mann-Whitney *U* test. Values of $P < .05$ were considered to indicate statistical significance.

RESULTS

PTCH1 mutations in the peripheral blood and KCOTs

A *PTCH1* mutation, c.1472delT, was detected in the peripheral blood as well as in the 2 KCOTs in the maxilla and mandible. Moreover, an additional *PTCH1* mutation, c.264_265insAATA, was found in the maxillary KCOT but not in the peripheral blood or mandibular KCOT (Fig. 2; Table II).

Immunopositivities for Ki-67 and cyclin D1, but not p53, in the KCOTs

The pathologic findings indicated KCOTs with a lining of parakeratinized squamous epithelium without rete ridges in both the maxilla and the mandible. The columnar cells of each basal layer were often crowded. No apparent differences were found between the maxillary and mandibular tumors (Fig. 3, *A* and *B*).

It has been reported that the epithelial lining of KCOTs associated with NBCCS exhibits overexpression of Ki-67, p53, and cyclin D1.[15,17] Both the maxillary and the mandibular KCOTs showed frequent immunopositivities for Ki-67 and cyclin D1, but sparse p53 immunopositivity, in our patient (Fig. 3, *C-H*). The Ki-67 LI was significantly higher in the maxillary KCOT (17.7%) than in the mandibular KCOT (14.3%; $P < .05$). Although the cyclin D1 LI was higher in the maxillary KCOT (15.1%) than in the mandibular KCOT (13.6%), the difference was not significant ($P > .05$; Table III).

DISCUSSION

The *PTCH1* gene is considered to be a tumor suppressor gene, because heterozygous loss of *PTCH1* is detected in certain sporadic and familial cases of basal cell carcinoma.[18,19] Although Knudson's "2-hit" theory[20] was proposed as a pathogenesis for KCOTs associated with NBCCS,[21] the molecular mechanism for how KCOTs develop in NBCCS patients is poorly understood. There have been a small number of reports on mutational analyses of sporadic and NBCCS-associated KCOTs.[22,23] However, pairwise mutational analyses of both tumor and nontumor tissues or analyses of multiple KCOTs derived from a single patient have rarely been reported.

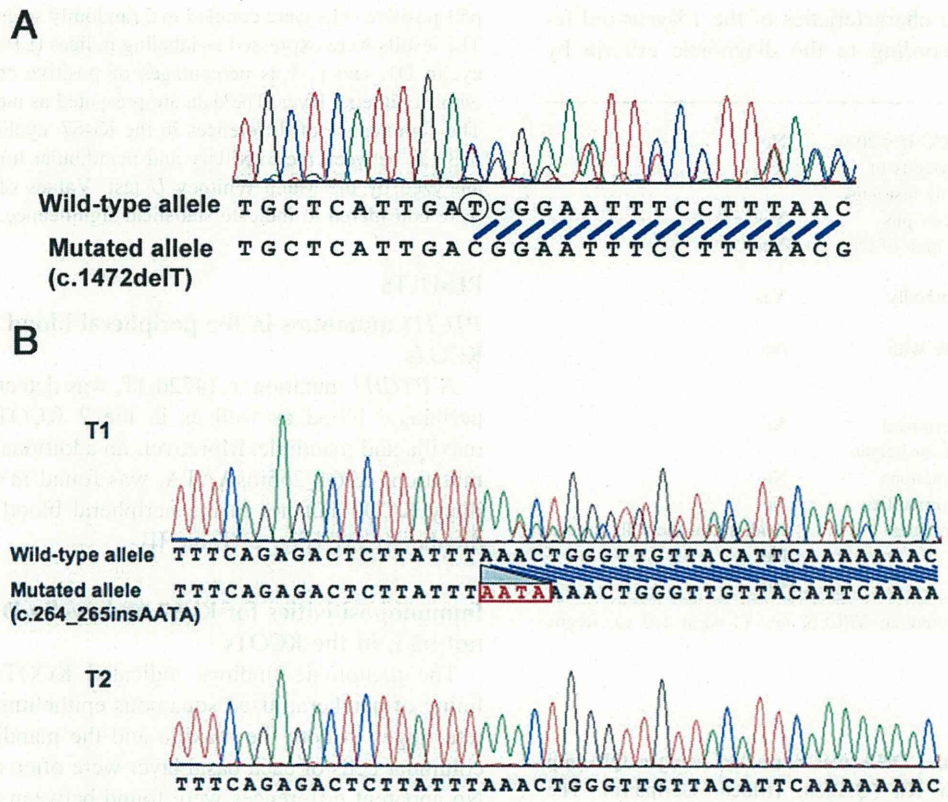

Fig. 2. Mutational analysis of the patient. **A,** A heterozygous deletion at nucleotide position 1472 of the *PTCH* gene (c.1472delT) is detected in the peripheral blood as well as in the 2 KCOTs removed from the maxilla and mandible. **B,** A heterozygous insertion between nucleotide positions 264 and 265 of the *PTCH1* gene (c.264_265insAATA) is detected in the maxillary tumor (T1). This mutation is not detected in the mandibular tumor (T2).

Table II. Summary of *PTCH1* mutation in peripheral blood and tumors

	Exon 2	*Exon 10*
Blood	—	c.1427delT
T1	c.264_265insAATA	c.1427delT
T2	—	c.1427delT

T1, Maxillary keratocystic odontogenic tumor; *T2,* mandibular keratocystic odontogenic tumor.

In the present study, we detected a germline mutation in a 15-year-old girl with NBCCS. Interestingly, an additional somatic mutation of a 4-bp insertion was found in the maxillary KCOT but not in the mandibular KCOT. It is unlikely that the absence of the additional mutation in the mandibular KCOT simply reflects the absence of tumor cells in the specimen, because both tumor samples contained similar amounts of KCOT cells. Since both mutations lead to truncation of the PTCH1 protein, which is deleterious for its function, the maxillary KCOT in this patient was thought to have developed because of complete loss of *PTCH1* function that resulted in constitutive activation of the SHH pathway. The mechanism for the tumor formation in the mandibular KCOT is currently unknown. Other components of the SHH pathway, such as *smoothened* and *suppressor of fused*, may be involved.[9] Nevertheless, it is intriguing that distinct somatic mutational events appear to be involved in the 2 tumors that developed simultaneously in this patient.

To address the question of whether the different somatic mutations led to different phenotypes in the 2 KCOTs, we performed immunohistochemical analyses of the tumors by using antibodies against proteins that are related to a poor prognosis for KCOTs.[13-16] Although the pathologic findings were similar between the 2 tumors, the LI of Ki-67, a proliferation marker, was significantly higher in the maxillary KCOT than in the mandibular KCOT. These observations are consistent with an earlier study in which *PTCH1* mutations were found to be related to epithelial cell proliferation in KCOTs.[24]

The p53 pathway was reported to synergize with the SHH pathway for the development of medulloblastoma

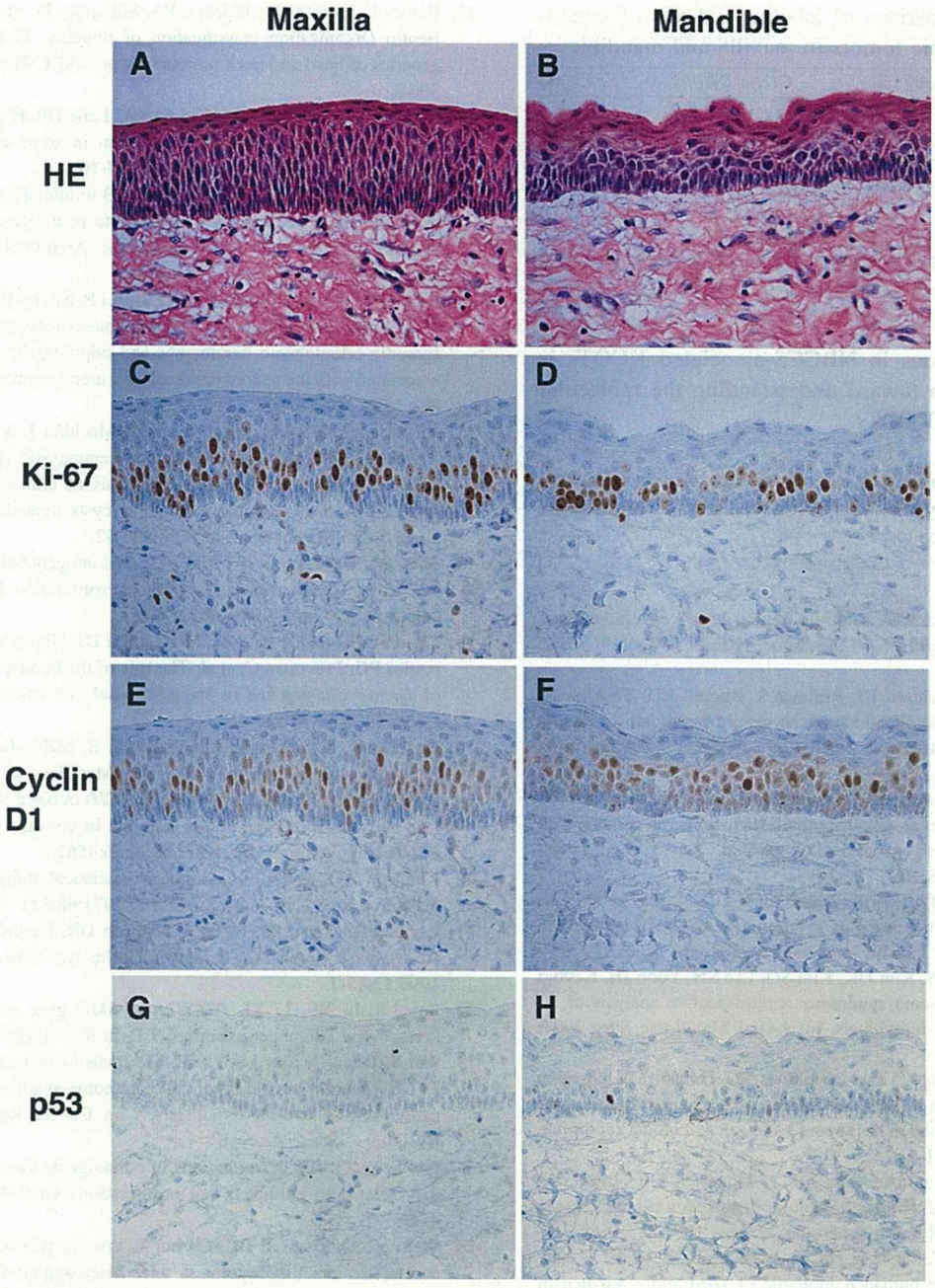

Fig. 3. Histopathologic features of the maxillary (**left**) and mandibular (**right**) keratocystic odontogenic tumors (KCOTs; magnification × 40). **A and B,** Hematoxylin-eosin (HE) staining shows a characteristic epithelial lining that is covered with parakeratinized squamous epithelium without rete ridges. **A,** Maxillary KCOT often exhibited crowded basal cell layer. **B,** KCOT with 6–8-cell layers, with palisaded basal cells. **C and D,** Ki-67–positive cells are stratified within basal and prickle cell layers. **E and F,** Cyclin D1–positive cells are mainly observed in the prickle cell layers. **G and H,** P53-positive cells are sparsely distributed.

associated with NBCCS in a mouse model, and p53 was also reported to be overexpressed in most NBCCS-associated KCOTs.[13,14,25] However, p53 staining was sparse in the samples from the present patient, indicating the absence of p53 mutations and suggesting that the p53 pathway was unlikely to be involved in this patient.

KCOTs were not considered to be tumors until recently. The accumulation of a spectrum of somatic and

Table III. Comparison of labeling indexes of keratocystic odontogenic tumors in maxilla and mandible

	Ki-67 (%)	*Cyclin D1 (%)*	*p53 (%)*
Maxilla	17.7 ± 3.9	14.3 ± 3.0	ND
Mandible	15.1 ± 3.2*	13.6 ± 1.4†	ND

Data are presented as mean ± SD and compared by unpaired *t* test.
ND, Not detected.
*$P < .05$ between maxilla and mandible.
†No significant difference between maxilla and mandible.

germline mutations in NBCCS-associated KCOTs is expected to help toward understanding the molecular pathogenesis of KCOTs.

The authors are indebted to the patient who participated in this study. They also thank Hiromi Hatsuse for excellent technical assistance.

REFERENCES

1. Gorlin RJ, Goltz RW. Multiple nevoid basal-cell epithelioma, jaw cysts and bifid rib. A syndrome. N Engl J Med 1960;262: 908-12.
2. Evans DGR, Ladusan EJ, Rimmer S, Burnell LD, Thakker N, Farndon PA. Complications of the nevoid basal cell carcinoma syndrome: results of the population based study. J Med Genet 1993;30:460-4.
3. Kimonis VE, Goldstein AM, Pastakia B, Yang ML, Kase R, DiGiovanna JJ, et al. Clinical manifestations in 105 persons with nevoid basal cell carcinoma syndrome. Am J Med Genet 1997;69:299-308.
4. Shanley S, Ratcliffe J, Hockey A, Haan E, Oley C, Ravine D, et al. Nevoid basal cell carcinoma syndrome: review of 118 affected individuals. Am J Med Genet 1994;50:282-90.
5. Ahn SG, Lim YS, Kim DK, Kim SG, Lee SH, Yoon JH. Nevoid basal cell carcinoma syndrome: a retrospective analysis of 33 affected Korean individuals. Int J Oral Maxillofac Surg 2004; 33:458-62.
6. Hahn H, Wicking C, Zaphiropoulous PG, Gailani MR, Shanley S, Chidambaram A, et al. Mutations of the human homolog of Drosophila patched in the nevoid basal cell carcinoma syndrome. Cell 1996;85:841-51.
7. Johnson RL, Rothman AL, Xie J, Goodrich LV, Bare JW, Bonifas JM, et al. Human homolog of patched, a candidate gene for the basal cell nevus syndrome. Science 1996;272:1668-71.
8. Fujii K, Kohno Y, Sugita K, Nakamura M, Moroi Y, Urabe K, et al. Mutations in the human homologue of *Drosophila patched* in Japanese nevoid basal cell carcinoma syndrome patients. Hum Mutat 2003;21:451-2.
9. Cohen MM. The hedgehog signaling network. Am J Med Genet 2003;123A:5-28.
10. Sasaki R, Saito K, Watanabe Y, Takayama Y, Fujii K, Agawa K, et al. Nevoid basal cell carcinoma syndrome with cleft lip and palate associated with the novel *PTCH* gene mutations. J Hum Genet 2009;54:7:398-402.
11. Morgan TA, Burton CC, Qian F. A retrospective review of treatment of the odontogenic keratocyst. J Oral Maxillofac Surg 2005;63:635-9.
12. Barnes L, Eveson JW, Reichart PA, Sidransky D, editors. World Health Organization classification of tumours. Pathology and genetics of head and neck tumours. Lyon: IARC Press; 2005. p. 306-7.
13. Ogden GR, Chisholm DM, Kiddie RA, Lane DP. P53 protein in odontogenic cysts: increased expression in some odontogenic keratocysts. J Clin Pathol 1992;45:1007-10.
14. Lombardi T, Odell EW, Morgan PR. P53 immunohistochemistry of odontogenic keratocysts in relation to recurrence, basal-cell budding and basal-cell naevus syndrome. Arch Oral Biol 1995; 40:1081-4.
15. Muzio LL, Staibano S, Pannone G, Bucci P, Nocini PR, Bucci E, et al. Expression of cell cycle and apoptosis-related proteins in sporadic odontogenic keratocysts and odontogenic keratocysts associated with the nevoid basal cell carcinoma syndrome. J Dent Res 1999;78:1345-53.
16. Kuroyanagi N, Sakuma H, Miyabe S, Machida J, A Kaetsu, M Yokoi, et al. Prognostic factors for keratocystic odontogenic tumor (odontogenic keratocyst): analysis of clinico-pathologic and immunohistochemical findings in cysts treated by enucleation. J Oral Pathol Med 2009;38:386-92.
17. Shear M. The aggressive nature of the odontogenic keratocyst: is it a benign cystic neoplasm? Part 2. Proliferation and genetic studies. Oral Oncol 2002;38:323-31.
18. Gailani MR, Stahle-Backdahl M, Leffell DJ, Glynn M, Zaphiropoulos PG, Pressman C, et al. The role of the human homologue of *Drosophila patched* in sporadic basal cell carcinomas. Nat Genet 1996;14:78-81.
19. Unden AB, Holmberg E, Lundh-Rozell B, Stahle-Backdahl M, Zaphiropoulos PG, Toftgard R, et al. Mutations in the human homologue of *Drosophila patched* (*PTCH*) in basal cell carcinomas and the Gorlin syndrome: different in vivo mechanisms of PTCH inactivation. Cancer Res 1996;56:4562-5.
20. Knudson AG. Mutation and cancer: statistical study of retinoblastoma. Proc Natl Acad Sci U S A 1971;68:823-30.
21. Levanat S, Gorlin RJ, Fallet S, Johnson DR, Fantasia JE, Bale AE. A two-hit model for defects in Gorlin syndrome. Nat Genet 1996;12:85-7.
22. Sun LS, Li XF, Li TJ. *PTCH1* and *SMO* gene alterations in keratocystic odontogenic tumors. J Dent Res 2008;87:575-9.
23. Pan S, Dong Q, Sun LS, Li TJ. Mechanisms of inactivation of *PTCH1* gene in nevoid basal cell carcinoma syndrome: modification of the two-hit hypothesis. Clin Cancer Res 2010;16: 442-50.
24. Pan S, Li TJ. *PTCH1* mutations in odontogenic keratocysts: are they related to epithelial cell proliferation? Oral Oncol 2009; 45:861-5.
25. Wetmore C, Eberhart DE, Curran T. Loss of p53 but not ARF accelerates medulloblastoma in mice heterozygous for patched. Cancer Res 2001;61:513-6.

Reprint requests:
Dr. Ryo Sasaki
Department of Oral and Maxillofacial Surgery
Tokyo Women's Medical University School of Medicine
8-1 Kawada-cho, Shinjuku-ku
Tokyo 162-8666
Japan
sasaki@oms.twmu.ac.jp

genesis 48:233–243 (2010)

ARTICLE

Zebrafish Gene Knockdowns Imply Roles for Human *YWHAG* in Infantile Spasms and Cardiomegaly

Yuta Komoike,[1] Katsunori Fujii,[2] Akira Nishimura,[3,4] Yoko Hiraki,[5] Michiko Hayashidani,[6] Keiko Shimojima,[1] Tsutomu Nishizawa,[1] Kouji Higashi,[2] Kumi Yasukawa,[2] Hirotomo Saitsu,[3] Noriko Miyake,[3] Takeshi Mizuguchi,[3] Naomichi Matsumoto,[3,4,7] Makiko Osawa,[8] Yoichi Kohno,[2] Toru Higashinakagawa,[9] and Toshiyuki Yamamoto[1]*

[1]International Research and Educational Institute for Integrated Medical Sciences (IREIIMS), Tokyo Women's Medical University, Tokyo, Japan
[2]Department of Pediatrics, Graduate School of Medicine, Chiba University, Chiba, Japan
[3]Department of Human Genetics, Graduate School of Medicine, Yokohama City University, Yokohama, Japan
[4]21st Century Center of Excellence (COE) Program of MEXT, The Yokohama City University, Yokohama, Japan
[5]Hiroshima Municipal Center for Child Health and Development, Hiroshima, Japan
[6]Medical Center for Premature and Neonatal Infants, Hiroshima City Hospital, Hiroshima, Japan
[7]Solution-Oriented Research for Science and Technology, Japan Science and Technology Agency, Tokyo, Japan
[8]Department of Pediatrics, Tokyo Women's Medical University, Tokyo, Japan
[9]Department of Biology, School of Education, Waseda University, Tokyo, Japan

Received 7 May 2009; Revised 21 December 2009; Accepted 28 December 2009

Summary: Williams-Beuren syndrome (WBS) is a neurodevelopmental disorder presenting with an elfin-like face, supravalvular aortic stenosis, a specific cognitive-behavioral profile, and infantile hypercalcemia. We encountered two WBS patients presenting with infantile spasms, which is extremely rare in WBS. Array comparative genomic hybridization (aCGH) and fluorescent in situ hybridization (FISH) analyses revealed atypical 5.7-Mb and 4.1-Mb deletions at 7q11.23 in the two patients, including the WBS critical region and expanding into the proximal side and the telomeric side, respectively. On the proximal side, *AUTS2* and *CALN1* may contribute to the phenotype. On the telomeric side, there are two candidate genes *HIP1* and *YWHAG*. Because detailed information of them was unavailable, we investigated their functions using gene knockdowns of zebrafish. When zebrafish *ywhag1* was knocked down, reduced brain size and increased diameter of the heart tube were observed, indicating that the infantile spasms and cardiomegaly seen in the patient with the telomeric deletion may be derived from haploinsufficiency of *YWHAG*. genesis 48:233–243, 2010. © 2010 Wiley-Liss, Inc.

Key words: Williams-Beuren syndrome (WBS); infantile spasms; cardiomegaly; *YWHAG*; *HIP1*; developmental delay; array comparative genomic hybridization (aCGH); fluorescent in situ hybridization (FISH); 7q11.23; microdeletion

INTRODUCTION

William-Beuren syndrome (WBS) is a recognizable malformation syndrome (MIM: 194050) (http://www.ncbi.nlm.nih.gov/Omim/) caused by hemizygosity of chromosome 7q11.23 (Ewart *et al.*, 1993). WBS patients show mental retardation with a specific cognitive-behavioral profile, supravalvular aortic stenosis, infantile hypercalcemia, a hoarse voice, and distinctive dysmorphic features including an elfin-like face and edematous eyes. The prevalence of WBS in the population is approximately one in 7,500–20,000 (Ewart *et al.*, 1993; Stromme *et al.*, 2002; Wu *et al.*, 1998). Almost all deletions of 7q11.23 in patients with WBS have arisen by de novo mechanisms. The phenotypes of WBS patients are caused by haploinsufficiency of the contiguous genes included in approximately 1.5 Mb or 1.9 Mb regions of 7q11.23, which is mediated by flanking low-copy repeats (LCRs), and are common among WBS patients (Morris, 2006). More than 20 genes are located within this common deletion region, including the elastin gene (*ELN*), the most important gene for the cardiovascular changes associated with WBS (Morris, 2006). Nucleotide sequence alterations in *ELN* can cause isolated supravalvular aortic stenosis (Morris, 2006).

Additional Supporting Information may be found in the online version of this article.

*Correspondence to: Toshiyuki Yamamoto, International Research and Educational Institute for Integrated Medical Sciences (IREIIMS), Tokyo Women's Medical University, 8-1 Kawada-cho, Shinjuku-ward, Tokyo 162-8666, Japan. E-mail: yamamoto@imcir.twmu.ac.jp

Contract grant sponsors: Program for Promoting the Establishment of Strategic Research Centers, Special Coordination Funds for Promoting Science and Technology, Ministry of Education Culture, Sports, Science and Technology (Japan).

Published online 9 February 2010 in Wiley InterScience (www.interscience.wiley.com).
DOI: 10.1002/dvg.20607

Patients with uncommon deletion sizes that also show atypical phenotypes are of particular interest to researchers for assessment of genotype-phenotype comparisons. WBS patients with common deletions rarely have epilepsy, especially infantile spasms. Until now, only a few WBS patients with infantile spasms have been reported (Mizugishi *et al.*, 1998; Morimoto *et al.*, 2003). In 2008, Marshall *et al.* reported 28 patients with infantile spasms, twenty of whom had deletion of 7q11.23, the WBS critical region, and eight of whom had deletion of 7q21. A genotype-phenotype analysis localized the shortest region of overlap to membrane associated guanylate kinase, ww and pdz domains-containin, 2 gene (*MAGI2*), located in the telomeric region outside of the WBS critical region (Marshall *et al.*, 2008). However, some WBS patients with infantile spasms had no deletion in *MAGI2*, and some patients with haploinsufficiency of *MAGI2* did not have infantile spasms. Thus, there may be other genes in this region that are responsible for infantile spasms.

Recently, we encountered two WBS patients, both of whom presented with infantile spasms, and one of whom also presented with cardiomegaly. Array comparative genomic hybridization (aCGH) showed that the 7q11 deletions in these patients are larger than the common WBS deletion, but do not include *MAGI2*. Thus, we investigated genes that might be responsible for such atypical phenotypes.

RESULTS

Patient Profiles

Patient 1. A boy was born at 41 weeks of gestation as a second child between an unrelated 33-year-old father and 31-year-old mother without any familial history. His birth weight was 2,892 g, length was 49 cm, and head circumference was 33 cm. He was transferred to the neonatal intensive care unit (NICU) because of poor sucking. He was suspected of WBS at one month, and fluorescent in situ hybridization (FISH) analysis confirmed a deletion in 7q11.23 (data not shown). Infantile spasm occurred at four months. An electroencephalogram revealed hypsarrhythmia. He was referred to us for evaluation of development. Specific facial features were noted, including wide forehead, broad eyebrows, downslanting palpebral fissures, inverted epicanthus, periorbital fullness, low-set ears with prominent lobes, short nose, full nasal tip, malar hypoplasia, long philtrum, thick lips, high arched palate, full cheeks, and micrognathia. Echocardiography revealed supravalvular aortic stenosis and peripheral pulmonary stenosis. Bilateral radioulnar synostosis, joint laxity, soft skin, bilateral inguinal hernia, left cryptorchidism, and spina bifida occulta were also noted. Hypercalcemia was not observed. Spasms were refractory to anticonvulsant drugs, but were well controlled with adrenocorticotrophic hormone (ACTH) therapy from 7 to 9 months. Mental development was severely retarded. At 21 months, he could not crawl or sit, and his developmental quotient (DQ) was 20. Abdominal ultrasonography, auditory brainstem response, and fundoscopy did not reveal any abnormality. Brain magnetic resonance imaging (MRI) implied atrophic brain (Supporting Information Fig. S1), which may have been caused by ACTH therapy.

Patient 2. A girl was born by normal vaginal delivery at term with a body weight of 2,600 g. Because of a moderate systolic murmur, she was examined, and cardiac hypertrophy and a prominent thick cardiac muscle were revealed by chest-X-ray and echocardiography (Supporting Information Figs. S2A, B), respectively. Heart catheterization revealed supravalvular aortic stenosis, peripheral pulmonary stenosis (Supporting Information Figs. S2C, D) and high pressure at 99 mmHg, 80 mmHg, 20 mmHg, and 39 mmHg, in the left ventricle, aorta, pulmonary artery, and right ventricle, respectively. She was treated with β-blockers without any arrhythmia and exacerbation of hypertrophic cardiomyopathy. She had characteristic facial features, with a wide large mouth and an elfin face. Conventional FISH analysis showed microdeletions in 7q11.23 (data not shown). At 18 months, she suffered serial tonic spasms more than 30 times per day. Electroencephalogram showed typical hypsarrhythmia (Supporting Information Fig. S2E) and MRI revealed normal structure and signal intensities in the brain (Supporting Information Figs. S2F, G). We first prescribed several antiepileptic drugs (i.e., sodium valproate, zonisamide and carbamazepine in turn), but these failed to decrease her epileptic attacks. Finally, we introduced ACTH therapy after obtaining informed consent from her parents. ACTH therapy provided successful control of her epileptic spasms, although some exacerbation of cardiac hypertrophy was observed.

Molecular Cytogenetic Analysis of Deletions

Because infantile spasms is a very rare complication for WBS patients, the deletion breakpoints of patient 1 and patient 2 were analyzed by aCGH.

In patient 1, BAC aCGH identified losses of genomic copy numbers of eight clones (Fig. 1A). Additional FISH analysis confirmed a 5.7-Mb deletion from RP11-134N6 to RP11-204E14 (UCSC Genome Browser assembly on Mar. 2006: nucleotides 68,597,691–74,341,149; Fig. 1B,C and Table 1). The deletion was not identified in the patient's parental chromosomes (data not shown) and included the common deletion region. The telomeric deletion breakpoint was localized to RP11-600I23, which exhibited weaker signal intensity on the deleted chromosome than on normal chromosome 7 (Fig. 1C). RP11-600I23 was exactly matched to telomeric LCR. No LCR-related structures were identified around the proximal deletion breakpoint.

In patient 2, oligo aCGH revealed a microdeletion of 7q11.23-q11.23 with a deletion size of 4.1-Mb (72,338,350-76,475,408; Fig. 2A,B). Two-color FISH analysis confirmed the deletion by the loss of the probe signal (Figs. 2C,D, Table 1).

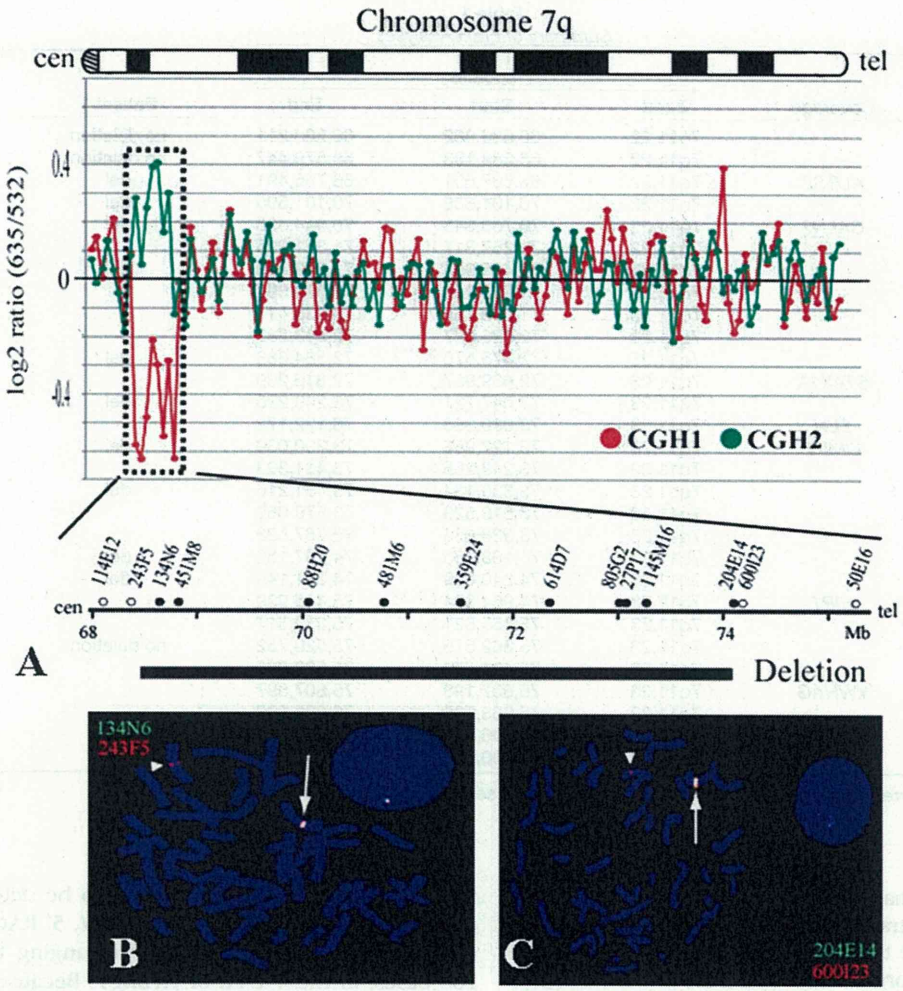

FIG. 1. Molecular cytogenetic analysis of the deletion of 7q11.23 in patient 1 using BAC aCGH and FISH analyses. **A:** aCGH analysis of chromosome 7q. Results are presented below the ideogram of 7q. Patient DNA labeled with Cy5 and normal control DNA labeled with Cy3 was used to obtain the CGH1 data (red), and the CGH2 data (green) was obtained using the same DNAs with the dye labels reversed. The dashed box indicates deleted clones, and is expanded below to give detailed information of the BAC clones used in this study (UCSC Genome Browser coordinates, build 36). Filled circles represent deleted BACs, and open circles represent clones that were not deleted. **(B, C)** Chromosomal FISH analyses. Arrows depict visible signals and arrowheads depict absence of signal.

Identification of Zebrafish *bip1*

Although several genes exist in the expanded deletion region of chromosome 7q11.23 in patient 2, there are two candidate genes normally expressed in the brain and therefore potentially responsible for the observed symptoms; i.e. tyrosine 3-monooxygenase/tryptophan 5-monooxygenase activation protein, gamma (14-3-3gamma; YWHAG) gene and the huntingtin-interacting protein 1 (HIP1) gene.

To study whether the deletion of these loci have any relation to infantile spasms and cardiomegaly, we used zebrafish as a model organism. In zebrafish, a homolog of mammalian *HIP1* has yet to be experimentally isolated, but its sequence has been predicted from genomic information. Therefore, for functional analysis, we cloned and identified the cDNA encoding zebrafish *bip1*. Using a reverse transcription (RT)-polymerase chain reaction (PCR)-based strategy, we obtained a full-length open reading frame (ORF) of zebrafish *bip1*, consisting of 3,141 bases and encoding 1,047 amino acids (Accession #AB494966). Zebrafish Hip1 protein has 70% identity to its human and mouse homologs. In addition, in silico software pfam analysis (http://pfam.sanger.ac.uk) revealed that zebrafish *Hip1* contains an N-terminal ANTH/ENTH domain and a C-terminal I/LWEQ domain, both of which are conserved in human *HIP1* (Bhattacharyya *et al.*, 2008). Collectively, these results suggest that *bip1* identified in this study is the zebrafish homolog of mammalian *HIP1* structurally and functionally.

Table 1
Summary of FISH Analyses

BAC clone	Coverage	Location			Patient 1	Patient 2
		Band	Start	End		
RP11-114E12		7q11.22	68,036,962	68,208,211	no deletion	
RP11-243F5		7q11.22	68,389,193	68,579,447	no deletion	
RP11-134N6	*AUTS2*	7q11.22	68,597,691	68,766,491	del	
RP11-88H20		7q11.22	70,101,386	70,101,595	del	
RP11-481M6	*CALN2*	7q11.22	70,766,345	70,944,325	del	
RP11-193J17		7q11.22	71,257,317	71,371,995		marker
RP11-359E24		7q11.22	71,495,966	71,682,413	del	
RP11-479C13		7q11.23	71,883,286	72,073.394		no deletion
RP11-396K3		7q11.23	71,903,765	72,538,417		no deletion
RP11-483G21		7q11.23	72,326,667	72,513,882		del
RP11-614D7		7q11.23	72,375,570	72,564,868	del	
RP11-622P13	*STAX1A*	7q11.23	72,639,987	72,819,209		del
RP11-805G2		7q11.23	73,047,721	73,249,220	del	
	ELN	7q11.23	73,080,363	73,122,172		
RP11-27P17	*LIMK1*	7q11.23	73,122,968	73,290,039	del	
RP11-7M12		7q11.23	73,249,265	73,431,303		del
RP11-1145M16		7q11.23	73,330,134	73,491,216	del	
RP11-247L6		7q11.23	73,510,529	73,676,067		del
RP11-137E8		7q11.23	73,528,656	73,767,523		del
RP11-201E14		7q11.23	74,108,105	74,267,152	del	
RP11-600I23		7q11.23	74,240,609	74,341,149	del	
RP11-99J9	*HIP1*	7q11.23	74,964,894	75,145,939		del
RP11-845K6		7q11.23	75,055,521	75,239,517		del
RP11-50E16		7q11.23	75,362,579	75,520,752	no deletion	
RP11-229D13		7q11.23	75,401,774	75,583,095		del
RP11-951G4	*YWHAG*	7q11.23	75,607,193	75,807,597		del
RP11-340A14		7q11.23	75,968,235	76,028,838		del
RP11-87O14		7q11.23	76,306,441	76,490,214		del
RP11-467H10		7q11.23	76,490,656	75,587,315		no deletion

Genome location corresponds to the March 2006 human reference sequence (NCBI Build 36).
del: deletion

For functional analysis of zebrafish *hip1*, we chose a gene knockdown strategy using morpholino antisense oligos (MOs). Because this approach requires precise nucleotide sequence information of the 5′-untranslated region (UTR), we performed 5′ rapid amplification of cDNA ends (RACE) to determine the sequence of the 5′-UTR of *hip1* in our zebrafish strain. Several nucleotide fragments, ranging from 121 to 264 bases, corresponding to the region upstream of the translation initiation ATG codon were obtained. The 121-base overlapping sequence of these clones was completely identical, and was of sufficient length to design two nonoverlapping, translation-inhibiting MOs (*hip1*-MO1 and *hip1*-MO2). A 5′-terminal guanine residue on the longest clone, rather than the observed thymine in the genomic sequence, suggested that this 264-bp clone contained the full-length 5′-UTR (Supporting Information Fig. S3). In addition, 386 bases of the 3′-UTR, including the polyadenylation signal and polyA tail, were also cloned. Overall, we identified the complete cDNA sequence of zebrafish *hip1*.

Sequence Analysis of 5′-UTR and Exon-Intron Junctions of Zebrafish *ywhag1*

Although a zebrafish homolog of human *YWHAG* was previously isolated and reported as *ywhag1* (Besser *et al.*, 2007; Pujic *et al.*, 2006; Woods *et al.*, 2005), the 5′-UTR in our zebrafish strain had to be determined to design MOs against zebrafish *ywhag1*. 5′ RACE revealed variation of sequence and length, ranging from 29 to 160 bases, in the 5′-UTR of *ywhag1*. Because the 5′ terminus of the shortest clone contained a guanine residue rather than the adenine residue identified in the other clones, this clone was identified as a full-length clone of the shortest form of the 5′-UTR (Supporting Information Fig. S4). To maximize the effect of the MOs, this shortest sequence was used as a template to design MOs that bind all transcripts of *ywhag1*.

Because the 5′-UTR we cloned was too short and not suited for MO binding, we obtained only one MO for translational inhibition of this gene (*ywhag1*-MO1). Because we needed another MO for splicing inhibition, genomic sequences at exon-intron boundaries were required. However, the whole sequence of *ywhag1* was splitted into two clones, Zv7_NA122 and Zv7_NA727, representing the 5′-terminal region (consisting of the 5′-UTR and the 5′ portion of the ORF [initiator ATG to 87G]) and the 3′-terminal region (the 3′ portion of the ORF [88G to the stop codon] and the 3′-UTR), respectively. According to the information in these sequences, zebrafish *ywhag1* was revealed to be composed of two exons and one intron (Supporting Information Fig. S5). Consequently, we cloned fragments containing the puta-

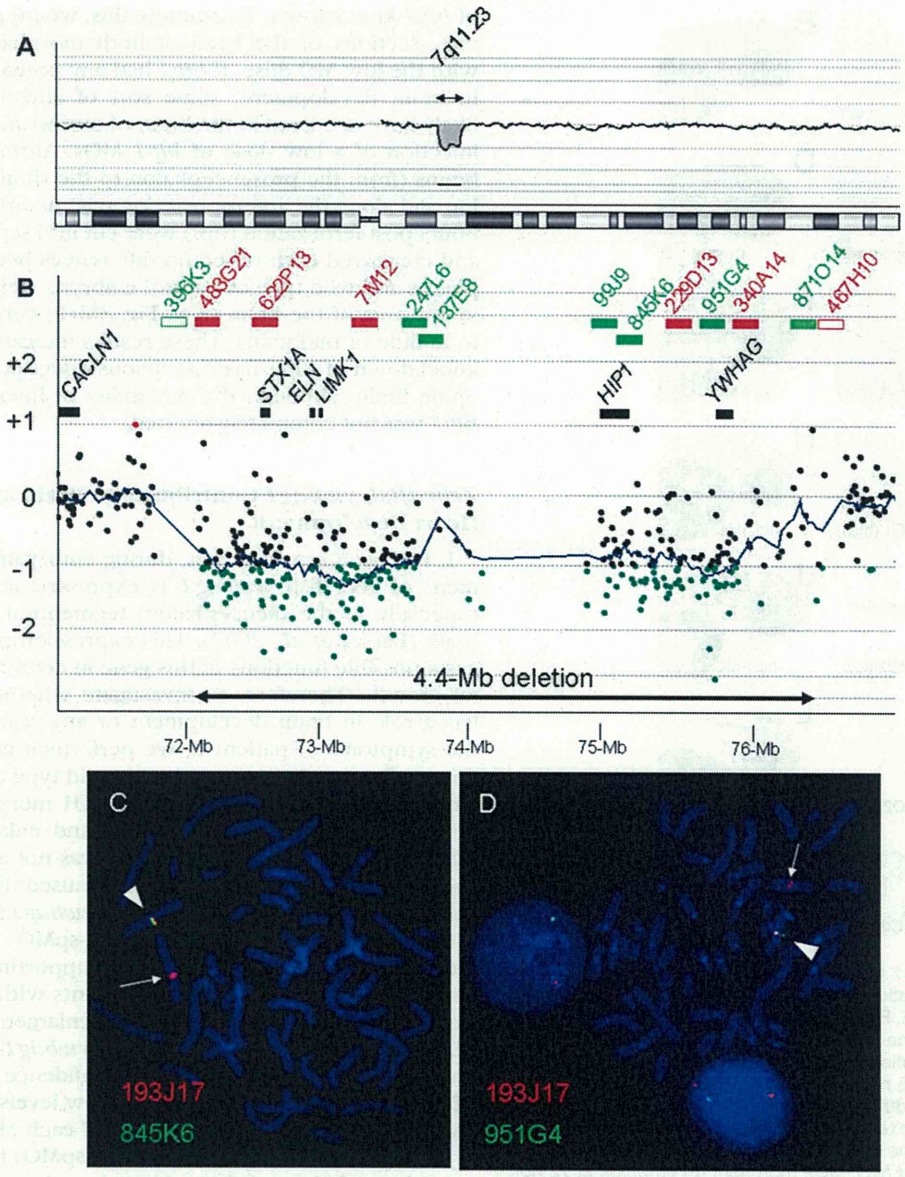

FIG. 2. Molecular cytogenetic analysis of the deletion of 7q11.23 in patient 2 using oligo array CGH and FISH analyses. **A:** Chromosome view indicating loss of genomic copy number in 7q11.23. **B:** Gene View indicating the range of the 4.1-Mb deletion (double-headed arrow, bottom). Black rectangles indicate the locations of known genes within the deletion region. Red and green rectangles indicate the locations of the BAC clones used for FISH analyses. Closed and open rectangles indicate deletion and no deletion, respectively. (C, D) FISH analyses indicating deletion of the green signals (arrows) of RP11-845K6 (C) and RP11-951G4 (D).

tive junction of exon 1/intron 1 and intron 1/exon 2 (Supporting Information Fig. S5), and designed *ywhag1*-spMO.

Zebrafish bip1 Plays No Obvious Role in Brain Development

To confirm whether the deletion of *HIP1* contributes to the phenotype of patient 2, we performed gene knockdown analysis of *bip1* in zebrafish. Microinjection of a small amount (3 ng) of *bip1*-MO1 reduced the yolk extension without any other remarkable phenotypes (Fig. 3E,F) compared with wild type and control MO-injected zebrafish (Fig. 3A–D). By a high dose (5 ng) injection of *bip1*-MO1, the morphants showed complete absence of yolk extension, a narrow body along the dorsoventral axis, and mandibular hypoplasia (Fig. 3G,H). To verify whether these phenotypes were specific for

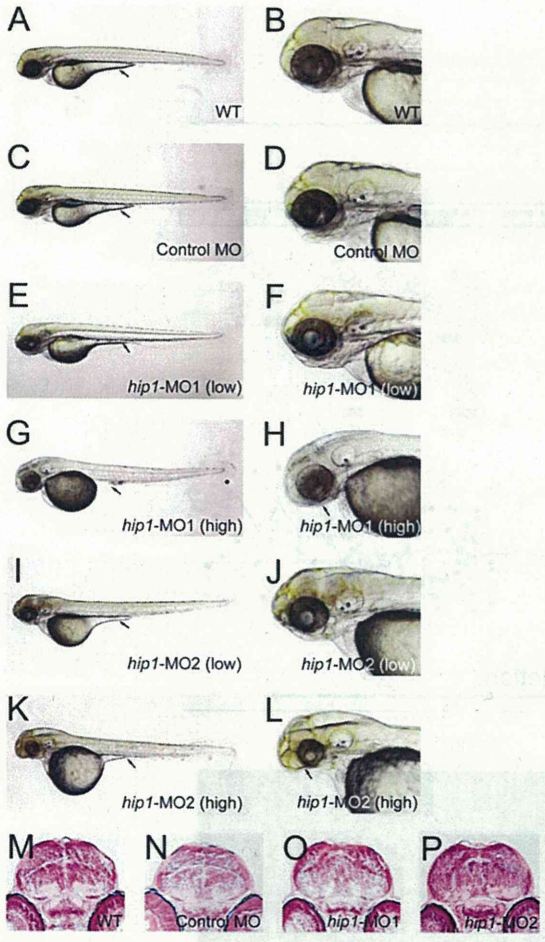

FIG. 3. Zebrafish *hip1* has no evident role in brain development. Morphological observation of wild type (WT) (**A**, **B**), control (**C**, **D**), *hip1*-MO1 morphant (E, F, G, H), and *hip1*-MO2 morphant (**I**, **J**, **K**, **L**) embryos at 72 hpf. Gene knockdown of *hip1* using a low dose (3 ng) of MOs caused reduction of yolk extension (arrow in A, C, **E**, I), whereas a high dose (5 ng) resulted in complete lack of yolk extension, narrow body width, and mandibular agenesis (**G**, **H**, K, L). Arrows indicate yolk extension (G, K) and diminished lower jaw (H, L). Cross-sections of the midbrain in wild type (**M**), control (**N**), *hip1*-MO1 morphant (**O**) and *hip1*-MO2 morphant (**P**) embryos at 72 hpf. All images are displayed with dorsal to the top; A-L are displayed with rostral to the left.

knockdown of *bip1*, the other translation-inhibiting MO, *bip1*-MO2, was used. Similar to *bip1*-MO1 morphants, *bip1*-MO2 morphants showed dose-dependent phenotypes, including reduced yolk extension with no other defects when 3 ng of *bip1*-MO2 was injected (Fig. 3I,J), and complete absence of yolk extension, narrow body along the dorsoventral axis, and severe mandibular aplasia when 5 ng of *bip1*-MO2 was injected (Fig. 3K, L). In addition to these common phenotypes, *bip1*-MO2 morphants also displayed dysplasia of the brain with low penetrance at the higher dose (Fig. 3L), suggesting that this cerebral defect was not the result of specific action of *bip1* knockdown. To examine this, we prepared serial cross-sections of the head of both morphants treated with the low MO dose. If *bip1* had any primary function in brain development, some sort of alteration would likely have occurred in the brain of morphants following injection of a low dose of *bip1* MOs. Although whole brains (from the prosencephalon to the rhombencephalon and along the anteroposterior axis) of embryos at 72 hours post-fertilization (hpf) were cut into serial sections and compared each other, no differences between morphants and wild type or control embryos were observed in any area of the brain (e.g., Fig. 3M–P; corresponding to middle of midbrain). These results indicate that gene knockdown of *bip1* has no obvious effect on the developing brain, although the possibility of involvement of *bip1* was not completely omitted.

Zebrafish ywhag1 Contributes to Brain and Heart Development

It has been reported that, during embryonic development of zebrafish, *ywhag1* is expressed in the head, especially in the diencephalon, tegmentum, and hindbrain (Besser *et al.*, 2007). This expression pattern suggests possible functions of this gene in cerebral and neural growth. Therefore, to investigate whether *ywhag1* has a role in brain development or any relationship to the symptoms of patient 2, we performed gene knockdown of *ywhag1*. Compared with wild type and control embryos (Fig. 4A–D), the *ywhag1*-MO1 morphants (Fig. 4E,F) showed hypomorphic heads and enlarged heart tubes, whereas trunk development was not affected. To confirm that these defects were caused by *ywhag1* knockdown, the splice-inhibiting *ywhag1*-spMO was used. Microinjection of *ywhag1*-spMO drastically reduced mRNA level of *ywhag1* (Supporting Information Fig. S6), and resulted in morphants with a severely hypomorphic head phenotype and enlargement of the heart tube (Fig. 4G,H) similar to *ywhag1*-MO1 morphants (Fig. 4E,F). To gain more confidence, we tested whether coinjection of two MOs at low levels elicits synergistic effect. The quarter amount of each MO (0.75 ng of *ywhag1*-MO1 and 1 ng of *ywhag1*-spMO) that did not cause any obvious defects (data not shown) was coinjected into embryos. Morphant coinjected with these two MOs (*ywhag1*-spMO1+spMO) showed similar phenotypes common to *ywhag1*-MO1- and *ywhag1*-spMO-morphants (Fig. 4I,J). This result indicated that these two MOs exerted the synergistic effect in coinjected embryos (*ywhag1*-spMO1+spMO), and that *ywhag1* is required for normal development of the brain and the heart.

For further investigation of the brain and the heart aberrations in the morphant embryos, serial sections of the head and the heart were examined. Based on the expression pattern of *ywhag1*, we focused on the brain sections containing the diencephalon and midbrain tegmentum (Besser *et al.*, 2007). Compared with wild type and control embryos (Fig. 4K–N), *ywhag1* morphants